DOI: 10.1002/eji.202149181 Eur. J. Immunol. 2021. 51: 2074–2085

Basic

European Journal of Immunology

Immunomodulation and immune therapies

Research Article

Immunological analysis of the murine anti-CD3-induced cytokine release syndrome model and therapeutic efficacy of anti-cytokine antibodies

Lise Nouveau, Vanessa Buatois, Laura Cons, Laurence Chatel, Guillemette Pontini, Nicolas Pleche and Walter G. Ferlin

Light Chain Bioscience-Novimmune S.A., Geneva, Switzerland

The aberrant release of inflammatory mediators often referred to as a cytokine storm or cytokine release syndrome (CRS), is a common and sometimes fatal complication in acute infectious diseases including Ebola, dengue, COVID-19, and influenza. Fatal CRS occurrences have also plagued the development of highly promising cancer therapies based on T-cell engagers and chimeric antigen receptor (CAR) T cells. CRS is intimately linked with dysregulated and excessive cytokine release, including IFN-γ, TNF-α, IL 1, IL-6, and IL-10, resulting in a systemic inflammatory response leading to multiple organ failure. Here, we show that mice intravenously administered the agonistic hamster anti-mouse CD3ε monoclonal antibody 145-2C11 develop clinical and laboratory manifestations seen in patients afflicted with CRS, including body weight loss, hepatosplenomegaly, thrombocytopenia, increased vascular permeability, lung inflammation, and hypercytokinemia. Blood cytokine levels and gene expression analysis from lung, liver, and spleen demonstrated a hierarchy of inflammatory cytokine production and infiltrating immune cells with differentiating organ-dependent kinetics. IL-2, IFN-γ, TNF-α, and IL-6 up-regulation preceded clinical signs of CRS. The co-treatment of mice with a neutralizing anti-cytokine antibody cocktail transiently improved early clinical and laboratory features of CRS. We discuss the predictive use of this model in the context of new anti-cytokine strategies to treat human CRS.

Keywords: Anti-CD3 · Anti-cytokine therapy · Cytokine release syndrome · Inflammatory cytokines · T-cell activation in vivo

Additional supporting information may be found online in the Supporting Information section at the end of the article.

Introduction

The 21st century has ushered in spectacular progress in the field of immunotherapy for cancer. T-cell engagers, immune checkpoint inhibitors, and chimeric antigen receptor (CAR) T cells represent a new era of remarkable therapeutic options extending life for cancer patients [1–3]. The pharmacology of these therapies, however, has at times led to severe cytokine release syndrome (CRS) and neurotoxicity [4]. Bach and colleagues first described a CRS following the administration of an agonistic anti-cluster differentiation 3 (CD3) mAb, OKT3, in patients undergoing renal transplantation [5], when excess TNF-α and IFN-γ was produced following the first injection of OKT3. This cytokine release, albeit transient, was characterized by high fever, headaches, and gastrointestinal symptoms. The syndrome's underlying "cytokine

Correspondence: Walter G. Ferlin
e-mail: walter.ferlin@lightchainbio.com

storm," the unrestrained release of proinflammatory mediators in response to a trigger, has also been seen across multiple infectious diseases including dengue [6,7], Lassa fever [8], Ebola [9], influenza [10,11], SARS, and in the recent COVID-19 outbreak [12,13]. Indeed, COVID-19-associated mortality is also characterized by excessive production of proinflammatory cytokines, thrombosis, and acute lung damage [13–17]. The CRS observed in all the above is often characterized by features seen in patients afflicted with hemophagocytic lymphohistiocytosis (HLH) and macrophage activation syndrome [18]. The recent approval for the use of mAbs blocking IFN-γ for primary forms of HLH [19] and IL-6 signaling in COVID-19 patients and following CAR T-cell treatments [20] is a clinical validation of cytokine storms causing CRS.

The cytokine storm induced in six healthy subjects in a 2006 Phase I clinical trial following administration of the CD28 superagonist antibody TGN1412 was the first demonstration of near-fatal consequences subsequent to excessive T-cell activation [21]. Within 90 min after a single i.v. dose of TGN1412, all six volunteers had a systemic inflammatory response characterized by the rapid induction of proinflammatory cytokines (especially IFN-γ and TNF-α), accompanied by other clinical manifestations of CRS, including nausea, diarrhea, erythema, vasodilatation, hypotension, and multiorgan failure [22].

In this study, we evaluated the role of proinflammatory cytokines up-regulated in an anti-CD3 mouse model of CRS leading to systemic inflammation and mortality. Mice administered the agonist anti-CD3ε antibody (herein called anti-CD3) developed an acute CRS characterized by weight loss, hepatosplenomegaly, leucopenia, and hemotoxicity. A single i.v. administration of anti-CD3 led to a rapid up-regulation of inflammatory mediators associated with T cell and macrophage activation. In particular, a sharp increase of TNF-α, IL-2, IL-6, and IFN-γ preceded the development of CRS features. We describe a hierarchical organ-dependent cytokine induction and production kinetics in the lung, the liver, and the spleen, driving the mobilization of a plethora of activated immune cells. CRS severity was particularly correlated with a prolonged neutrophil and macrophage infiltration in the lung. Coadministration of a neutralizing anti-cytokine antibody cocktail, targeting TNF-α, IL-2, IL-6, and IFN-γ, reduced early features of CRS, including body weight loss, prostration, piloerection, and hemotoxicity, as well as lung inflammation. However, the protection afforded by the anti-cytokine cocktail was not extended beyond 24 h after administration. These data suggest that early monitoring of blood biomarkers in CRS-susceptible patients may help identify risk profiles and those who might benefit from a multispecific neutralizing antibody-based treatment, an approach that may be applicable to a plethora of infectious and inflammatory diseases driven by a T-cell-mediated cytokine storm.

Results

Clinical and laboratory features of CRS resulting from CD3 agonism in mice

T-cell activation after in vivo administration of anti-CD3 to mice, results in increased cytokine secretion and extramedullary hematopoiesis in the spleen, was described over 30 years ago by Bluestone and colleagues [23]. We reproduced this model to dissect and comprehensively describe the clinical and laboratory features of CRS induced by CD3 agonism.

Within 2 h post anti-CD3 injection (2 hpi), the first symptoms, including piloerection and prostration, were observed in 20% of mice. At 6 hpi, 50% of the mice exhibited signs of clinical illness reaching a peak at 24 hpi with animals presenting also significant body weight loss and splenomegaly (Table 1 and Fig. 1A and B). Acute leucopenia (Fig. 1C), evidenced by a marked lymphopenia (Fig. 1D), was observed within 30 min after anti-CD3 injection lasting up to 24 hpi. The transient recovery in leucocyte count between 4 and 8 hpi was surprisingly correlated with an acute and transient neutrophilia (Fig. 1E). Monocyte count also increased at 6 hpi and remained above baseline levels for at least 48 hpi (Fig. 1F). A short-lived decrease in platelet numbers (Fig. 1G) with a concurrent increase in RBC counts occurred within the first hours post anti-CD3 injection, with an unexpected RBC drop 24 hpi with return to baseline levels (Fig. 1H). At the 5 μg anti-CD3 dose tested here, mice started to recover 48 hpi.

CD3 agonism leads to systemic hypercytokinemia with organ-specific cytokine production kinetics

Here, we describe a model of CRS caused by the activation of T cells leading to hypercytokinemia within the first hours following anti-CD3 injection. Th1 cytokines IFN-γ and IL-2 were rapidly

Table 1. Anti-CD3-injected mice present clinical features of CRS and anti-cytokine antibody cocktail alleviated early signs

		Hours post anti-CD3 injection (hpi)						
		0.5	1	2	6	24	48	72
Anti-CD3 + PBS	Piloerection	No	Low	Low	Medium	High	Medium	Low
	Prostration (% of mice)	0%	0%	20%	50%	100%	30%	0%
Anti-CD3 + anti-cytokines	Piloerection	No	No	No	No	High	Medium	Low
	Prostration (% of mice)	0%	0%	0%	0%	90%	30%	0%

Mice were injected with 5 μg of anti-CD3 plus PBS or plus an anti-cytokine cocktail. Data representative of N = 3 independent experiments with n = 5 mice per time point per experiment.

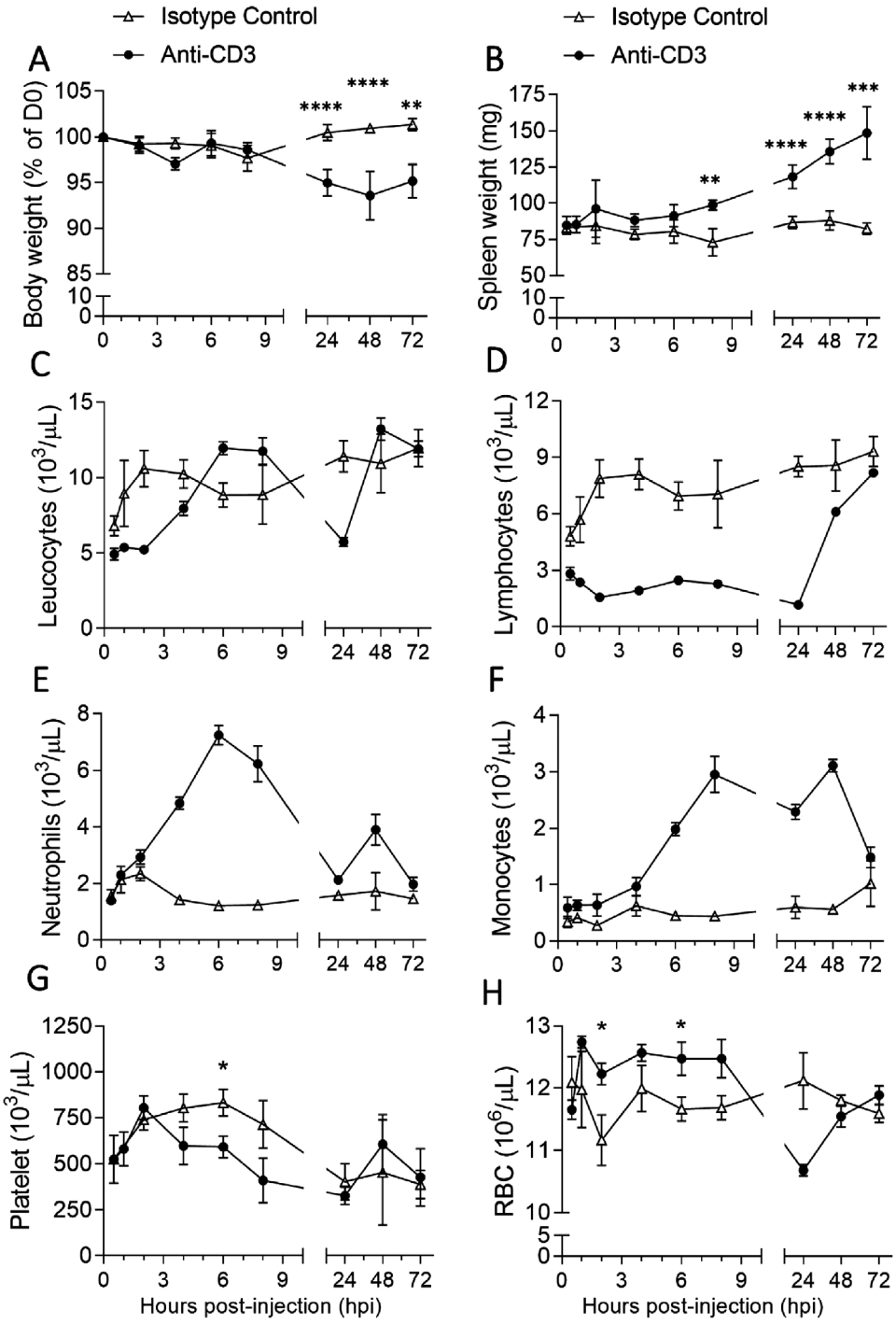

Figure 1. Clinical and laboratory features of CRS resulting from CD3 agonism in mice. Mice were injected i.v. with 5 μg of anti-CD3 or with 5 μg of isotype control. Body (**A**) and spleen (**B**) weight follow-up. Blood parameters including leucocyte (**C**), lymphocyte (**D**), neutrophil (**E**), monocyte (**F**), platelet (**G**), and RBC (**H**) counts. n = 4-15 mice per time point from N = 3 independent experiments. $^{*}p < 0.05$, $^{**}p < 0.01$, $^{***}p < 0.001$, and $^{****}p < 0.0001$ were obtained using the unpaired *t*-test. Values are displayed as mean ± SEM.

(i.e. 0.5 hpi) up-regulated in the blood to 40- and 10-fold levels above isotype control-injected mice (Table 2 and Fig. 2A and B), respectively. Cytokines often associated with macrophage activation syndrome, TNF-α and IL-6, were also rapidly up-regulated, with the former reaching a 75-fold peak at 1 hpi (Table 2 and Fig. 2C and D). These four cytokines were significantly up-regulated before the appearance of clinical symptoms (Table 1). The peak levels of IL-2 and IL-6 were observed at 2 hpi, with a 1200-fold (3500 pg/mL) and 300-fold (7500 pg/mL) increases, respectively and decreasing at 6 hpi (Table 2 and Fig. 2B and C).

In contrast, IFN-γ persisted at peak levels of 2000 pg/mL 6 hpi, a 2600-fold increase above baseline (Table 2 and Fig. 2A). Accordingly, IFN-γ-induced proteins CXCL9 and CXCL10 were also up-regulated, peaking at 6 and 2 hpi, respectively (Table 2 and Fig. 2F and G). Often described as anti-inflammatory, IL-10 was observed to be rapidly up-regulated within 1 hpi and peaked at 6 hpi, with a 80-fold increase above control (baseline) levels (Table 2 and Fig. 2E). Unexpectedly, only moderate increases in IL-1β (two fold increase) and IL-12p40 (18-fold increase) were observed at 1 and 2 hpi, respectively (Table 2). Inflammatory mediators frequently associated with macrophage activation and neutrophilia, including peaks of GM-CSF (1 hpi, 23-fold increase), CCL4/MIP-1β (2 hpi, 17-fold increase), and CXCL1 (2 hpi, 34-fold increase), were differentially up-regulated (Table 2 and Fig. 2H to J). The hypercytokinemia was accompanied by *de novo* mRNA synthesis in the spleen, the liver, and the lung (Fig. 2K-S). Interestingly, an organ-specific inflammatory gene signature was observed. The liver was the site where an increased gene expression profile was observed for *Ifn-γ* (Fig. 2K) and related *Cxcl9* and *Cxcl10* genes (Fig. 2P and Q), as well as *Tnf-α* (Fig. 2N), *Cxcl1* (Fig. 2R) and IL-6-induced protein *Saa* (Fig. 2S), but interestingly not *Il-6* (Fig. 2E). Indeed, the latter was instead significantly up-regulated in the spleen and in the lung following anti-CD3 administration (Fig. 2M). The spleen was the main site where *Il-2* gene up-regulation was observed (Fig. 2L), whereas *Il-10* was significantly up-regulated in the lung (Fig. 2O) as well as, albeit earlier, *Cxcl9, Cxcl10, Il-6*, *Saa*, and *Il-2* (Fig. 2L, M, P, Q, and S).

Mobilization of inflammatory cells after CD3 activation in vivo

The organ-specific cytokine signature, the drop in circulating lymphocyte count, and the increase in neutrophil and monocyte counts following anti-CD3 administration, suggested a potential differential mobilization of immune cells to the respective tissues. To further investigate this, the spleen, lungs, and liver were excised at 24 and 48 hpi (corresponding to peak of illness and initiation of recovery) and the infiltrating immune cells characterized (see Supporting information Fig. S1 to S4 for gating strategies). We noted a decrease in the proportion of $CD4^+$ and $CD8^+$ T cells in the spleen and lungs from mice treated with anti-CD3 although a marginal increase in the liver was observed at 24 hpi (Fig. 3A and E). The lung and spleen T cells were activated, as characterized by an up-regulation of CD25 and CD69 (Fig. 3B, C, F, G) and the down-regulation of CD62L at 24 hpi (Fig. 3D and H). Hepatic $CD8^+$ T cells, on the other hand, showed an increased expression of CD62L at 24 hpi (Fig. 3D and H). At 48 hpi however, overall, the $CD4^+$ and $CD8^+$ T cell proportions and activation state returned to normal levels (Fig. 3A-H). In addition, the proportion of NK cells increased in the liver, whereas a decrease was observed in the spleen and lung following anti-CD3 injection (Fig. 3I). On the other hand, myeloid subsets also fluctuated significantly in the studied organs. The frequency of neutrophils was increased in all three organs analyzed at 24 hpi, returning to basal levels in the spleen and the liver 48 hpi while remaining elevated in the lungs (Fig. 3J). A decrease in macrophage numbers was observed in the spleen and the liver whereas in lung, the frequency of alveolar-macrophages and interstitial-macrophages increased at 24 hpi, respectively (Fig. 3K). Taken together, systemic T-cell activation in vivo resulted in a cytokine and chemokine cascade driving the mobilization of a plethora of activated immune cells to the lung, liver, and spleen.

An anti-cytokine antibody cocktail alleviated early signs of CRS

We next tested if a cocktail of neutralizing antibodies targeting up-regulated cytokines (IL-2, IL-6, IFN-γ, and TNF-α) would ameliorate the anti-CD3-induced CRS in mice. To this end, anti-CD3 mice were co-treated with a combination of anti-cytokine mAbs

Table 2. Anti-CD3 injection induced a hypercytokinemia

	Hours post anti-CD3 injection (hpi)						
	0.5	1	2	6	24	48	72
IFN-γ	**40** ± 3.0	**459** ± 55	**1 410** ± 436	**2 610** ± 346	**359** ± 56	**13.5** ± 3	**2** ± 0.7
IL-2	**10** ± 1.4	**1 193** ± 106	**1 264** ± 338	**308** ± 50	**1** ± 0	**1** ± 0.1	**1** ± 0.1
TNF-α	**22** ± 1.2	**75** ± 4	**45** ± 8	**21** ± 1	**5.5** ± 1.2	**2** ± 1	**1** ± 0
IL-6	**3** ± 0.9	**118** ± 21	**306** ± 91	**88** ± 27	**17** ± 5	**2.5** ± 1.5	**0.2** ± 0.1
CXCL9	**1** ± 0.1	**2** ± 0.4	**16** ± 3	**131** ± 23	**44** ± 3	**10** ± 1.2	**3** ± 0.3
CXCL10	**1** ± 0.1	**8** ± 1	**22** ± 2	**20** ± 1	**8.5** ± 1.2	**3.5** ± 0.3	**1.5** ± 0.1
IL-10	**2** ± 0.4	**23** ± 3	**58** ± 15	**82** ± 6	**12** ± 3	**3** ± 2	**0.4** ± 0.1
IL-1β	**1** ± 0.1	**2** ± 0.3	**1.5** ± 0.3	**1** ± 0.03	**1** ± 0	**1.5** ± 0.5	**1** ± 0
IL12p40	**6** ± 4.9	**1** ± 1	**18** ± 11	**6** ± 2.5	**1** ± 0	**1** ± 0	**1** ± 0
GM-CSF	**5** ± 3.3	**23** ± 2.6	**11** ± 4	**4** ± 2.4	**1** ± 0.0	**1** ± 0.1	**1** ± 0
CCL4	**2** ± 0.3	**14** ± 1.7	**17** ± 4	**8.** ± 1.3	**1.5** ± 0.1	**1** ± 0.1	**0.5** ± 0.1
CXCL1	**3** ± 1.4	**30** ± 6	**34** ± 7	**24** ± 3	**21** ± 1.4	**0.7** ± 0.1	**0.5** ± 0.1

Mice were injected with 5 μg of anti-CD3. Plasma concentration of cytokines was quantified using a multiplex assay using Luminex. Fold increase above baseline (i.e. mean of plasma levels from isotype control injected mice) was calculated. Data are indicated as mean ± SEM.

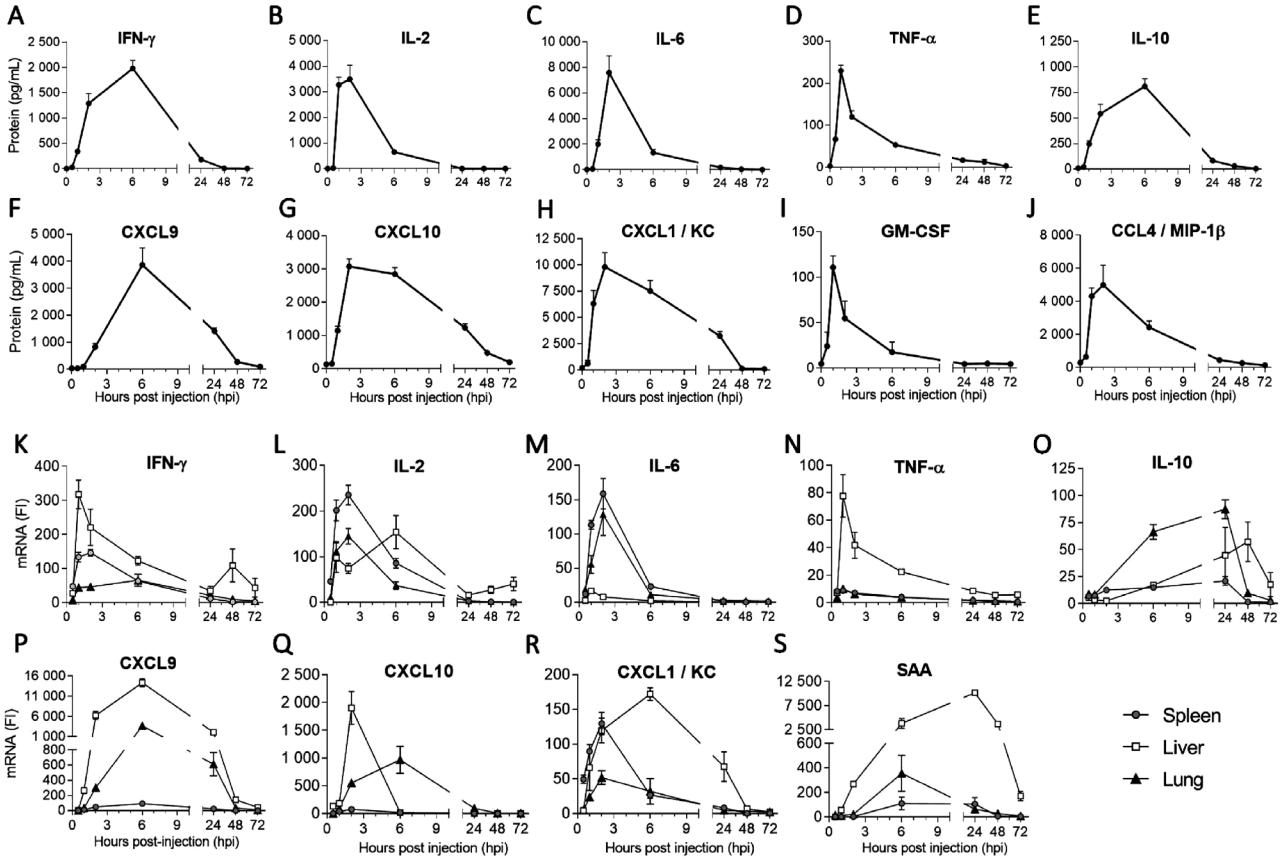

Figure 2. Anti-CD3-induced CRS leads to systemic hypercytokinemia with an organ-specific cytokine production kinetics. Mice were injected i.v. with 5 μg of anti-CD3 or isotype control. Graphs **A-J** represent Luminex-based quantification of plasma cytokines and chemokines. The baseline (t = 0 h) corresponds to the mean of isotype control injected mice. Graphs **K-S** represent the quantification of tissue-derived cytokine and chemokine mRNA levels evaluated by qPCR in the organs, expressed as fold increase above baseline. For plasma and spleen qPCR data, n = 9-10 from N = 2 independent experiments; for lungs and liver qPCR data n = 4-5 mice per time point from a single experiment. Values are displayed as mean ± SEM.

(anti-IL-2, -IL-6, -IFN-γ, -TNF-α mAbs). Mice administered the anti-cytokine antibody cocktail presented no clinical signs of CRS for up to 6 hpi, in contrast to 50% of the animals injected with anti-CD3 alone, who showed piloerection and prostration (Table 1). The severity of acute leucopenia, thrombocytopenia, erythrocytosis, and body weight loss seen in anti-CD3- treated mice was also significantly improved by the anti-cytokine antibody cocktail, while neutrophilia and monocytosis remained unchanged (Fig. 4A and B). As a measure of increased vascular permeability [24], Angiopoietin-2 (Ang-2) was up-regulated in anti-CD3-treated mice and was significantly reduced by the anti-cytokine cocktail (Fig. 4C). Analysis of bronchoalveolar lavage (BAL) also confirmed the amelioration in inflammatory parameters afforded by the anti-cytokine antibody cocktail (Fig. 4D and E). Here, cytokine blockade resulted in a decreased activation marker MHCII on F4/80$^+$ macrophages in the BAL at 24 hpi (Fig. 4D) and decreasing levels of inflammatory chemokines CXCL1 and CXCL10 (Fig. 4E). G-CSF was surprisingly up-regulated in the BAL in all treated groups (Fig. 4E). Interestingly, while G-CSF and CXCL1 are described to enhance neutrophil attraction, survival, and proliferation, this population was significantly diminished in the BAL across all treated groups (Fig. 4D) while an increase was observed in whole-lung cell suspensions (Fig. 3J). While the anti-cytokine antibody cocktail alleviated early signs of CRS, this was no longer the case 24 h post anti-CD3 injection. Nonetheless, the anti-cytokine cocktail afforded an increased benefit as compared to the monotherapy administration of the anti-cytokine mAbs (see Supporting information Table S1).

CRS severity is associated with sustained neutrophil and monocyte infiltration in lungs

To further understand the mechanisms underpinning CRS severity, we analyzed mice treated with a low (5 μg) or high (25 μg) dose of anti-CD3. Body weight loss, temperature loss, hepatomegaly and, to a lesser extent, splenomegaly aggravated in high-dose anti-CD3- treated mice (Fig. 5A to D). Indeed, while the low-dose anti-CD3 mice recovered spontaneously, mice receiving 25 μg anti-CD3 were sacrificed at 72 hpi for ethical reasons. Interestingly, the two anti-CD3 doses induced equivalent levels of hypercytokinemia (Fig. 5E and Supporting

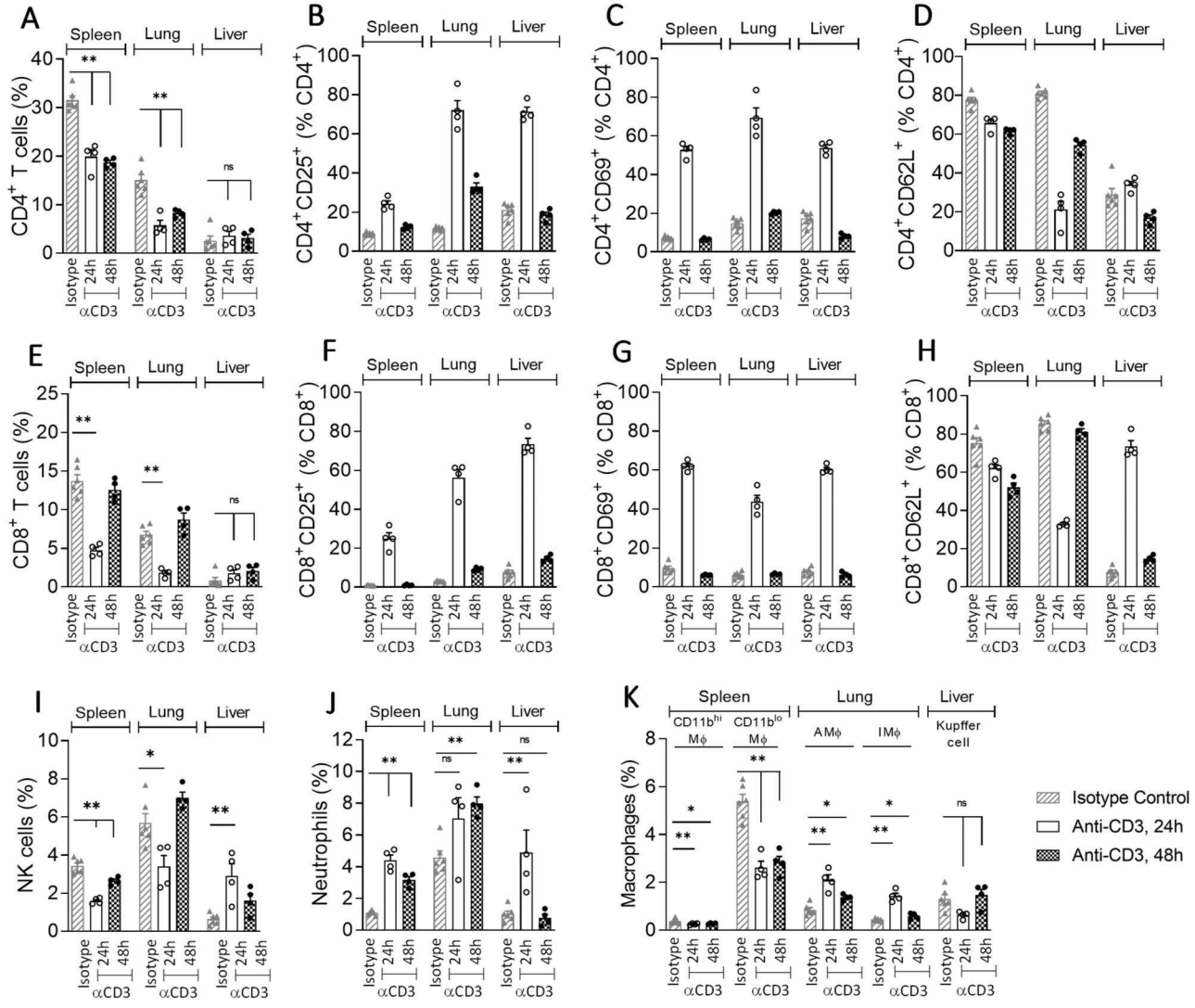

Figure 3. Organ-specific mobilization of inflammatory cells after CD3 activation. Mice were injected i.v. with 5 μg of anti-CD3 or with 5 μg of isotype control. Single cell-suspensions from the spleen, liver, and lungs were prepared 24 or 48 h postinjection, followed by immunophenotyping. Bar graphs **A** and **E** represent frequencies of $CD4^+$ and $CD8^+$ T cells expressed as percentage of total viable cells and up-regulation of CD25, CD69, and CD62L markers on $CD4^+$ (**B** & **D**) and $CD8^+$ (**F**-**H**) T cells. Plot **I** shows frequencies of NK cells and plots **J** and **K** show frequencies of myeloid cells expressed as a percentage of viable cells. Gating strategies and relative number of cells are available in Supporting information Fig. S1 to S4 and Supporting information Table S5. NK, natural killer; Mϕ, macrophages; AMϕ and IMϕ, alveolar and interstitial macrophages. Representative data of N = 2 independent experiments, n = 4-6 mice/organ per time point. $^*p < 0.05$, $^{**}p < 0.01$, and $^{***}p < 0.001$ as determined by one-tailed nonparametric Mann–Whitney U *t*-test. Values are displayed as the mean ± SEM.

information Table S2), whereas clinical signs of CRS (piloerection and prostration) occurred earlier and were more severe in mice given the higher dose. Blood levels of IFN-γ, TNF-α, and CXCL9 were still detectable in mice developing severe CRS at 48 hpi (Supporting information Table S2). Significant differences were observed only for circulating levels for IL-6 and CXCL1 at 48 hpi, when they were 25- and 30-fold higher, respectively, in high-dose anti-CD3- treated mice (Fig. 5E and Supporting information Table S2). Mobilization of inflammatory cells in tissues was equivalent across the two dose levels, normalizing at 48 hpi (see Supporting information Fig. S2 and S3 for gating strategies). Nonetheless, notable differences were observed in the proportions of lung monocytes and neutrophils (Fig. 5F). Indeed, the neutrophils in the severe form of CRS remained significantly higher at 48 hpi as compared to the low-dose anti-CD3- treated mice. In addition, this sustained increase correlated with an equally persistent elevated plasma concentration of CXCL1 (Fig. 5E). Similarly, $Ly6C^{low}$ resident monocytes were significantly persistent in lungs from severe CRS-afflicted mice (Fig. 5F). We next attempted to deplete neutrophils or macrophages to further investigate their contribution to the anti-CD3-induced CRS. While the anti-Ly6G antibody significantly depleted neutrophils from the lung and the spleen, only a 60% reduction was achieved in the liver. The treatment failed to significantly reverse CRS in mice

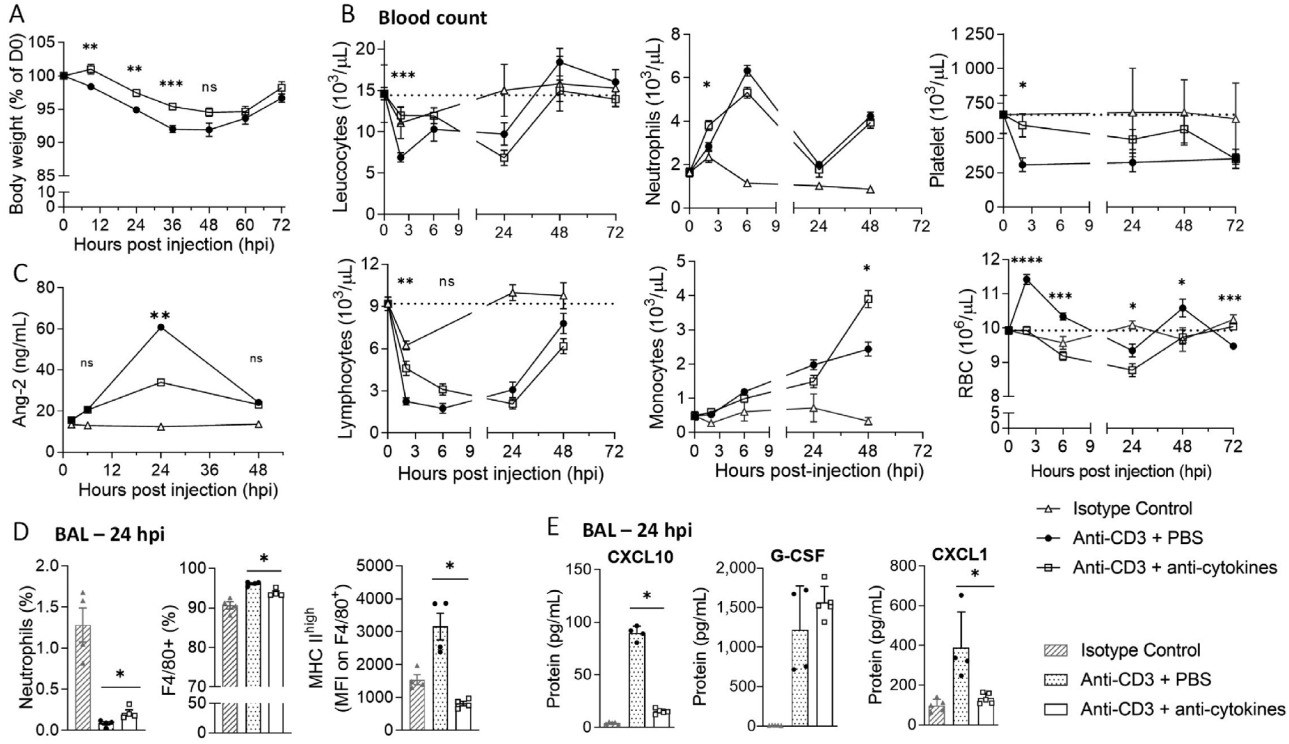

Figure 4. An anti-cytokine antibody cocktail alleviates early signs of CRS. Mice were i.v. co-injected with 5 µg of anti-CD3 plus either control PBS or an anti-cytokine cocktail (composed of an anti-IL-2, -IL-6, -IFN-γ, and -TNF-α mAbs, 30 mg/kg each), or with 5 µg of isotype control. Graphs show body weight (**A**) and blood parameters blood cell counts (**B**). Plasma concentration of Angiopoietin-2 (Ang-2) was determined by ELISA (**C**). Frequencies of neutrophils and F4/80$^+$ cells were expressed as percentage of viable cells (**D**). Cytokine concentrations were quantified in BAL at 24 hpi (**E**). RBC, red blood cell. n = 8-10 mice per time point, data from N = 2 independent experiments, except for **C** and **E** n = 4-5 mice per time point, data from a single experiment. $^*p < 0.05$, $^{**}p < 0.01$, $^{***}p < 0.001$, and $^{****}p < 0.0001$ as determined by one-tailed nonparametric Mann–Whitney U *t*-test. Values are displayed as the mean ± SEM.

(Supporting information Fig. S5). On the other hand, while clodronate liposome treatment was very efficient at depleting macrophages from the spleen and liver, it was ineffective at diminishing the cells from the lung. Here too, the treatment failed to reverse the anti-CD3-induced CRS (Supporting information Fig. S6). Taken together, data highlight a potential role of neutrophils and monocytes/macrophages in the physiopathology of severe CRS.

Discussion

In this study, an agonistic anti-CD3 was used to mimic severe forms of CRS induced by polyclonal T-cell activation in mice. Within 60 min and up to 24 hpi, a rapid and severe lymphopenia, erythrocytosis, thrombocytopenia, and neutrophilia was observed in mice following anti-CD3 injection. Interestingly, monocytosis occurred in mice, whereas monocytopenia was reported in healthy volunteers given the superagonist CD28 antibody TGN1412 [22]. These divergent responses could be explained by the differentiating ability to engage FcγRs of a hamster IgG1-Fc domain of the anti-CD3 in mice, as compared to the attenuated human IgG4 domain of TGN1412 in humans. Akin to CRS in mice, however, monocytosis, neutrophilia, and a marked lymphopenia were observed in patients severely ill with SARS-Cov-1 and -2 infections [25, 26]. In parallel, an induction of hypercytokinemia, characterized by type I cytokines and anti-inflammatory type II cytokines, was observed in mice. Of note, an up-regulation of CXCR3 ligands, CXCL9 and CXCL10, was seen in blood and in tissues of anti-CD3-treated mice within 1 hpi.

IFN-γ has been described as a main contributor to CRS in a plethora of preclinical models leading to sharp increases in CXCL9/CXCL10 [7,18,26,27]. Elevated levels of IFN-γ-induced chemokines have also been measured in patients with SARS and HLH [27–29]. IFN-γ is central to CpG-induced CRS in mice [30] and we have shown that tissue-derived levels of the cytokine are 500- to 2000-fold higher in organs than those measured in the blood [18]. Likewise, CXCL9/CXCL10 levels in pediatric secondary HLH patients correlated with key disease parameters and severity [18]. In the present study, type I cytokines *Tnf*-α, *Ifn*-γ, *Cxcl10*, and *Cxcl9* were rapidly induced in the liver following anti-CD3 administration. Within the first hpi, *de novo Ifn*-γ gene transcript levels peaked in the liver and spleen but to a lesser extent in the lung, with blood levels of the cytokine climaxing at 6 hpi. Interestingly, a second *Ifn*-γ spike was observed at 48 hpi only in the liver and correlated with a second wave of neutrophils in blood. While an IFNγ-mediated role in recruitment of neutrophils is described [31], the role for these cells in the CRS manifestations

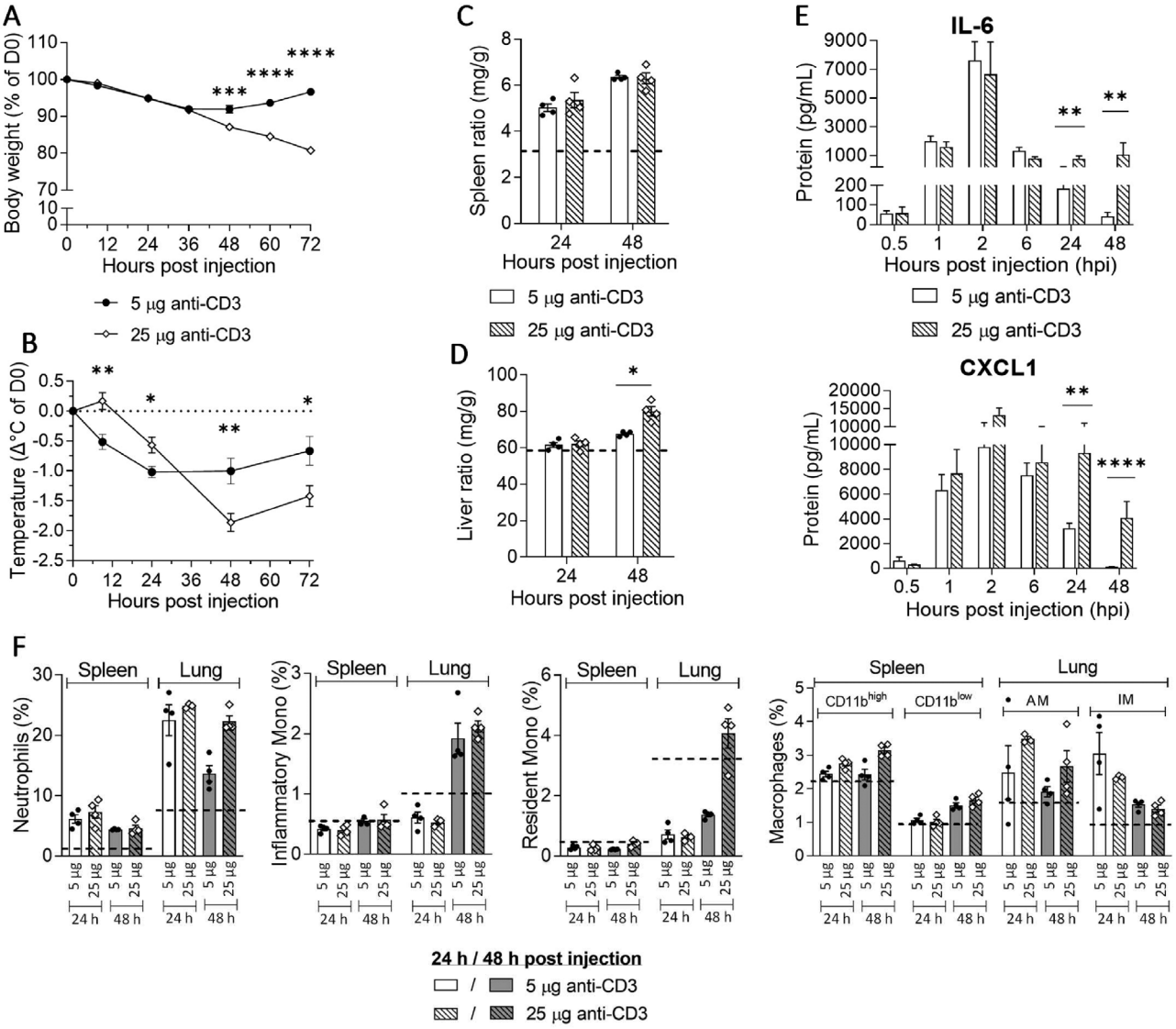

Figure 5. CRS severity is associated with sustained neutrophil and monocyte infiltration in lungs. Mice were i.v. injected with either 5 µg or 25 µg of anti-CD3. Body weight (**A**), temperature (**B**), spleen/body weight ratio (**C**), liver/body weight ratio (**D**), and IL-6 and CXCL1 plasma concentration (**E**) is shown. Immunophenotyping of single-cell suspensions from the spleen and the lungs (**F**). Gating strategies and relative number of cells are available in supporting information Fig. S2 and S3 and Table S5. Dotted lines on graphs in (**C**), (**D**), and (**F**) represent the mean of corresponding values of isotype control injected mice. n = 9-10 per time point from N = 2 independent experiments, except for C, D, and F n = 4-5 mice per time point, data from a single experiment representative of three experiments. $^{*}p < 0.05$, $^{**}p < 0.01$, $^{***}p < 0.001$, and $^{****}p < 0.0001$ as determined by one-tailed nonparametric Mann–Whitney U *t*-test. Values are displayed as the mean ± SEM.

described here remain unclear. Indeed, the co-administration of a neutrophil-depleting antibody, anti-Ly6G, failed to significantly reverse CRS features in mice. Nonetheless, a contribution of neutrophils to the anti-CD3-induced CRS manifestations should not be discounted, as the depleting efficacy of anti-Ly6G was not absolute, as evidenced here and by others [32]. As neutrophils have been shown to be important mediators of tissue damage in inflammatory diseases, potentially detrimental in the pathophysiology of COVID-19 [33], we do not rule out a pathogenic role for these cells in the anti-CD3-induced CRS in mice. The significant increase of *Ifn-γ* in the liver within minutes post anti-CD3 injection resulted in the local and sustained production of CXCL9 and CXCL10 as evidenced in the protein exudates and mRNA transcript up-regulation. As a consequence, CXCR3-expressing neutrophils [34], macrophages [35, 36], T cells [37], and NK cells [38] rapidly infiltrated the liver. While *Cxcl10* returned to baseline levels more rapidly, *Cxcl9* production was sustained at 2000-fold levels above homeostatic levels at 24 hpi in the liver.

Lungs from anti-CD3-treated mice presented a rapid and prolonged induction of proinflammatory cytokines/chemokines. Within 1 hpi, *Ifn-γ* production was increased 40-fold coinciding with a subsequent 3600-fold induction of *Cxcl9* and 1000-fold induction of *Cxcl10* mRNA transcripts with the former remaining at that level for at least 24 h. CXCL9/10 protein levels in the

lung remained high up to 48 hpi, certainly accounting for the infiltration of CXCR3-expressing neutrophils and activated T cells. CXCL1 and G-CSF may also induce significant neutrophil recruitment to the lung [39, 40], the BAL from anti-CD3-treated mice presented with high levels of these soluble factors, contributing to the sustained neutrophil infiltration at 48 hpi.

Severe CRS disease manifested by fever and pneumonia, leading to acute respiratory distress syndrome (ARDS) has been described in up to 20% of COVID-19 patients [41]. Additionally, CRS is common in patients with COVID-19 where elevated plasma IL-6 correlated with respiratory failure, ARDS, and adverse clinical outcomes [42,43]. High plasma levels of IL-6, CXCL10, GM-CSF, and increased lung neutrophil infiltrate, hallmarks of ARDS [44], were observed in our animal study as well as an increased proportion of activated alveolar macrophages ($MHCII^{high}$). Significant neutrophil and macrophage infiltration is also observed in pulmonary interstitium and alveoli from SARS-induced ARDS patients [26]. Interestingly, a prolonged neutrophil and monocyte infiltration in the pulmonary interstitium, but not in the alveoli, was observed in our study. In contrast to ARDS patients, we failed to observe histological differences in terms of lung architecture, cellularity in the alveolar cavities and interalveolar septal walls. This observation contrasted with the erythrocytosis and thrombocytopenia observed, thought to indicate disseminated intravascular coagulation and/or capillary leakage and also seen in humans administered Muromonab-CD3 or TGN1412 [22, 45]. Nonetheless, elevated Ang-2 plasma concentration in anti-CD3-treated mice suggests endothelial dysfunction and increased vascular permeability disorders [46]. Up-regulated levels of plasma Ang-2 is observed in COVID-19 and ARDS patients and correlated with mortality in the latter [16, 24, 47].The use of anti-cytokine approaches to manage CRS is validated by recent approvals of tocilizumab (anti-IL6R) and emapalumab (anti-IFN-γ) by the US Food and Drug Administration in the context CAR-T-cell-therapy and primary HLH [48, 49], respectively. Additionally, clinical trials with therapies, including a device designed to remove cytokines from blood using hemadsorption [50] and the blockade of IL-1 [51], GM-CSF, [52] and JAK1/JAK2 signaling [53,54], are ongoing. To this end, our anti-cytokine Ab cocktail, targeting IFN-γ, IL-6, TNF-α, and IL-2 (herein called anti-cytokine cocktail) reduced the clinical features of CRS induced by anti-CD3 injection in the first 24 hpi including body weight, prostration, and piloerection. Blood parameters remained in normal ranges in mice co-treated with the anti-CD3 and the anti-cytokine cocktail although neutrophilia and monocytosis persisted. Ang-2 plasma levels were significantly reduced by the anti-cytokine cocktail suggesting a reduction in vascular leakage supported by observed improvements in RBC and platelet counts. In addition, the lung inflammation induced by anti-CD3 treatment was improved as shown by the reduced BAL levels of CXCL1 and CXCL10, and decreased MHCII expression on alveolar macrophages. The anti-cytokine cocktail afforded an increased benefit as compared to the monotherapy administration of the anti-cytokine mAbs. Nonetheless, the benefit of the anti-cytokine cocktail was transient. A second injection of the cocktail at 12 hpi of anti-CD3 failed to prolong the protective benefit. IL-1 receptor antagonist, Anakinra®, or an anti-IL-15 neutralizing mAb (clone AIO.3, BioXCell) offered no improvement to the anti-cytokine cocktail. The failure to control CRS features beyond the initial 24 h post anti-CD3 administration was unexpected. In a mouse model recapitulating key features of CAR-T-cell-mediated CRS and neurotoxicity, human monocytes were the major source of IL-1 and IL-6 [55]. Accordingly, the authors observed that the syndrome was prevented by monocyte depletion or IL-6 blockade, but the latter failed to protect mice from delayed lethal neurotoxicity caused by meningeal inflammation. Anakinra®, however, diminished CRS and neurotoxicity, a finding corroborated by others [51]. The challenge to interrupt a cytokine storm by targeting IL-6 was made more evident in a recent clinical study where tocilizumab was ineffective at reducing COVID-19 mortality [56]. Nonetheless, co-administration of TNF-α and IFN-γ-neutralizing antibodies provided superior protection over monotherapy in a mouse SARS-CoV-2 infection model, highlighting a benefit of anti-cytokine combination therapy [14]. The limited benefit we observed in anti-CD3-treated mice by the cytokine-blocking antibody cocktail, and from efforts by others depleting inflammatory cells, parallel challenges faced in the clinical setting with patients suffering from severe forms of CRS. While cytokine activity was ablated by the high-dose antibody therapy we used in mice, cellular infiltration was not entirely abrogated. While clodronate liposome treatment was very efficient at depleting macrophages from spleen and liver, the treatment was ineffective at diminishing the cells from the lung. We cannot rule out a role for macrophages as their capacity for proinflammatory cytokine production have been shown to promote further leucocytosis and immune cell infiltrates in COVID-19- induced lung damage [57]. Similarly, we saw in our severe CRS model (using a higher dose of anti-CD3), increased body weight loss and an acute decrease in body temperature, confirming a critical role for the increased presence of neutrophils and macrophages in the lung.

The severe CRS induced by in vivo T-cell activation after anti-CD3 administration to mice highlights the central role of the subsequent cytokine storm and recruitment of pathogenic neutrophils and macrophages. The challenges encountered to halt disease relate to the complexities of severe T-cell-mediated CRS, while potentially advocating an anti-cytokine therapy as a therapeutic option for less-severe cases.

Materials and methods

Mice

All animal procedures were performed in accordance with the Swiss Veterinary Office guidelines and authorized by the Cantonal Veterinary Office. Studies were conducted with 6- to 8-week-old male BALB/cByJ, mice obtained from Charles River Laboratories (Saint-Germain-Nuelles, France). The animals were reared under conventional conditions temperature-controlled room (25 ± 2°C) under a 12 h light/dark cycle.

Antibodies used for in vivo studies in mice

The anti-CD3ε (hamster IgG), clone 145-2C11) mAb and the anti-IL2 (Rat IgG2a, clone JES6-1A12), anti-IFN-γ (Rat IgG1, clone XMG1.2) and anti-TNF-α (Rat IgG1, clone XT3.11) neutralizing mAbs were obtained from BioXCell (Lebanon, NH, USA). The Armenian hamster IgG isotype control (clone HTK888) was obtained from BioLegend® (CA, USA). The anti-IL6 neutralizing mAb, clone 1F7 [58], was produced inhouse.

Mouse model of CRS

Mice were injected i.v. with a single 5 μg anti-CD3 mAb, unless otherwise mentioned. Neutralizing mAbs were injected i.v. at 30 mg/kg simultaneously with the anti-CD3 mAb. At indicated time points, mice were euthanized by CO_2 inhalation, unless indicated. Blood cell count was performed with a ProCyte Dx analyzer (IDEXX Laboratories, Inc., ME, USA) or with a Hemavet analyzer (Drew Scientific, FL, USA). Samples of spleen, lung, and liver tissue were stored in RNA later (Sigma-Aldrich, St.-Louis, MO, USA) for gene expression analysis. Whole-lung, -liver, and -spleen were harvested for immune cell infiltration analysis.

Bronchoalveolar lavages analysis

Mice were sacrificed by lethal injection of pentobarbital (Streuli Pharma AG, Uznach, Switzerland). Bronchoalveolar lavage (BAL) was performed twice with sterile PBS. BAL fluids were centrifuged, supernatants were kept at −20°C for cytokines analysis and cell pellets were resuspended for immunophenotyping analysis.

Measurement of cytokines and chemokines in plasma

The plasma concentrations of cytokines and chemokines were measured using MILLIPLEX MAP multiplex immunodetection kits (Merck Millipore, Burlington, MA, USA) and analyzed on the Luminex® 200™ immunoassay analyzer (Luminex®, TX, USA), according to manufacturer's instructions. Plasma level of Ang-2 was quantified with the Ang-2 Mouse ELISA Kit (Abcam, Cambridge, UK) according to manufacturer's instructions.

Gene expression

Spleen, liver, and lung RNA isolated using RNeasy mini-Kit (Qiagen, Hilden, Germany) was reverse transcribed using High-Capacity cDNA Reverse Transcription kit (Applied Biosystems®, Foster City, CAL, USA). Quantitative PCR (qPCR) was performed using SYBR® Green Master Mix (Applied Biosystems®) on the 7900HT Fast Real-Time PCR System from Applied Biosystems®. The $\Delta\Delta Ct$ method was used to calculate the relative gene expression levels (RQ) with β-actin gene as housekeeping gene. The primer sequences are listed in Supporting information Table S3.

Cell preparation

Single-cell suspension of liver was performed using a dissociation kit (Miltenyi Biotec, Bergisch Gladbach, Germany) and the gentleMACS™ Dissociator (Miltenyi Biotec) according to the manufacturer's protocol. Single-cell suspension from spleen and lungs were prepared by enzymatic digestion in collagenase IV (Gibco) and DNase I (Sigma-Aldrich) for 20 min at 37°C, followed by mechanical digestion with the gentleMACS™ Dissociator (Miltenyi Biotech). RBC lysis was performed using ACK buffer (Ammonium-Chloride-Potassium). Cell suspensions were filtered through a 70 μM Nylon filter (BD Falcon™) and counted using a cell viability analyzer (Vi-CELL XR, Beckman Coulter, CAL, USA).

Flow cytometry

After cells were counted, 2×10^6 cells per sample were stained with Fixable Viability Stain 620 (BD Biosciences) according to manufacturer's instructions. Cells were then incubated with Mouse BD Fc Block™ and surface staining was directly performed in the dark for 20 min at 4°C (see Supporting information Table S4 for a list of antibodies, clones, fluorochromes, manufacturers). Cells were then washed twice with FACS buffer and acquired on the CytoFLEX S flow cytometer (Beckman Coulter). Data analyses were performed using FlowJo software (Tree Star Inc., OR, USA). Flow cytometry experiments were done in accordance with the guidelines of the journal [59].

Statistical analysis

GraphPad Prism (GraphPad Software, CA, USA) was used for all statistical analysis. The unpaired *t*-test or one-tailed nonparametric Mann–Whitney U *t*-test were used for statistical comparison. *p*-value of <0.05 was considered significant.

Acknowledgments: The authors would like to thank Drs. X. Chauchet, E. Hatterer, and D. Merkler, for scientific input and the former for help in the setup of flow cytometry panels; Y.R. Donati for BAL and lung perfusion methodologies and E. Eggimann for animal husbandry.

Conflict of Interest: The authors declare no commercial or financial conflict of interest.

Author Contributions: VB and WGF designed and conceived the project. LN and WGF analyzed the data and wrote the manuscript. LN, LCo, and LCh performed the mouse experiments. GP produced the antibody and NP performed the analytics. LN performed in vitro experiments and prepared the figures for the manuscript. All the authors revised the manuscript and approved the final version.

Peer review: The peer review history for this article is available at https://publons.com/publon/10.1002/eji.202149181.

Data availability statement: Data available on request from the authors.

References

1 **Zhang, Y.** and **Zhang, Z.**, The history and advances in cancer immunotherapy: understanding the characteristics of tumor-infiltrating immune cells and their therapeutic implications. *Cell. Mol. Immunol.* 2020. **17**: 807–821

2 **Robert, C.**, A decade of immune-checkpoint inhibitors in cancer therapy. *Nat. Commun.* 2020. **11**: 3801.

3 **Gupta, S.**, **Gupta, S. C.**, **Hunter, K. D.** and **Pant, A. B.**, Immunotherapy: a new hope for cancer patients. *J. Oncol.* 2020. https://doi.org/10.1155/2020/3548603

4 **Shimabukuro-Vornhagen, A.**, **Gödel, P.**, **Subklewe, M.**, **Stemmler, H. J.**, **Schlößer, H. A.**, **Schlaak, M.**, **Kochanek, M.** et al., Cytokine release syndrome. *J. Immunother. Cancer.* 2018. **6**: 56

5 **Chatenoud, L.**, **Ferran, C.**, **Legendre, C.**, **Thouard, I.**, **Merite, S.**, **Reuter, A.**, **Gevaert, Y.** et al., In vivo cell activation following OKT3 administration. Systemic cytokine release and modulation by corticosteroids. *Transplantation*. 1990. **49**: 697–702

6 **Srikiatkhachorn, A.**, **Mathew, A.** and **Rothman, A. L.**, Immune-mediated cytokine storm and its role in severe dengue. *Semin. Immunopathol*. 2017. **39**: 563–574.

7 **Patro, A. R. K**, **Mohanty, S.**, **Prusty, B. K.**, **Singh, D. K.**, **Gaikwad, S.**, **Saswat, T.**, **Chattopadhyay, S.** et al., Cytokine signature associated with disease severity in dengue. *Viruses*. 2019. **11**: 34.

8 **Prescott, J. B.**, **Marzi, A.**, **Safronetz, D.**, **Robertson, S. J.**, **Feldmann, H.** and **Best, S. M.**, Immunobiology of Ebola and Lassa virus infections. *Nat. Rev. Immunol.* 2017. **17**: 195–207

9 **Wauquier, N.**, **Becquart, P.**, **Padilla, C.**, **Baize, S.** and **Leroy, E. M.** Human fatal zaire ebola virus infection is associated with an aberrant innate immunity and with massive lymphocyte apoptosis. *PLoS Negl. Trop. Dis*. 2010. **4**: e837.

10 **Tisoncik, J. R.**, **Korth, M. J.**, **Simmons, C. P.**, **Farrar, J.**, **Martin, T. R.** and **Katze, M. G.**, Into the eye of the cytokine storm. *Microbiol. Mol. Biol. Rev.* 2012. **76**: 16–32

11 **Liu, Q.**, **Zhou, Y. -H.** and **Yang, Z. -. Q.**, The cytokine storm of severe influenza and development of immunomodulatory therapy. *Cell. Mol. Immunol.* 2016. **13**: 3–10

12 **Mehta, P.**, **Mcauley, D. F.**, **Brown, M.**, **Sanchez, E.**, **Tattersall, R. S.** and **Manson, J. J.**, COVID-19: consider cytokine storm syndromes and immunosuppression. *Lancet North Am. Ed.* 2020. **395**: 1033–1034

13 **Vaninov, N.**, In the eye of the COVID-19 cytokine storm. *Nat. Rev. Immunol.* 2020; 277.

14 **Karki, R.**, **Sharma, B. R.**, **Tuladhar, S.**, **Williams, E. P.**, **Zalduondo, L.**, **Samir, P.**, **Zheng, M.** et al., Synergism of TNF-α and IFN-γ triggers inflammatory cell death, tissue damage, and mortality in SARS-CoV-2 infection and cytokine shock syndromes. *Cell* 2020. **184**:149-168.

15 **Huang, C.**, **Wang, Y.**, **Li, X.**, **Ren, L.**, **Zhao, J.**, **Hu, Yi**, **Zhang, Li** et al., Clinical features of patients infected with 2019 novel coronavirus in Wuhan, China. *Lancet North Am. Ed.* 2020. **395**: 497–506.

16 **Smadja, D. M.**, **Guerin, C. L.**, **Chocron, R.**, **Yatim, N.**, **Boussier, J.**, **Gendron, N.**, **Khider, L.** et al., Angiopoietin-2 as a marker of endothelial activation is a good predictor factor for intensive care unit admission of COVID-19 patients. *Angiogenesis* 2020. **23**: 611–610.

17 **Gibson, P. G.**, **Qin, L.** and **Puah, S. H.**, COVID-19 acute respiratory distress syndrome (ARDS): clinical features and differences from typical pre-COVID-19 ARDS. *Med. J. Aust.* 2020. **213**: 54–56.

18 **Buatois, V.**, **Chatel, L.**, **Cons, L.**, **Lory, S.**, **Richard, F.**, **Guilhot, F.**, **Johnson, Z.** et al., Use of a mouse model to identify a blood biomarker for IFNγ activity in pediatric secondary hemophagocytic lymphohistiocytosis. *Transltinl. Res.* 2017. **180**: 37–52.

19 **Locatelli, F.**, **Jordan, M. B.**, **Allen, C.**, **Cesaro, S.**, **Rizzari, C.**, **Rao, A.**, **Degar, B.** et al., Emapalumab in children with primary hemophagocytic lymphohistiocytosis. *N. Engl. J. Med.* 2020. **382**: 1811–1822.

20 **Neelapu, S. S.**, **Tummala, S.**, **Kebriaei, P.**, **Wierda, W.**, **Gutierrez, C.**, **Locke, F. L.**, **Komanduri, K. V.** et al., Chimeric antigen receptor T cell therapy: assessment and management of toxicities. *Nat. Rev. Clin. Oncol.* 2018. **15**: 47–62.

21 **Hünig, T.**, The storm has cleared: lessons from the CD28 superagonist TGN1412 trial. *Nat. Rev. Immunol.* 2012. **12**: 317–318.

22 **Suntharalingam, G.**, **Perry, M. R.**, **Ward, S.**, **Brett, S. J.**, **Castello-Cortes, A.**, **Brunner, M. D.** and **Panoskaltsis, N.**, Cytokine storm in a phase 1 trial of the anti-CD28 monoclonal antibody TGN1412. *N. Engl. J. Med.* 2006. **355**: 1018–1028.

23 **Hirsch, R.**, **Gress, R. E.**, **Pluznik, D. H.**, **Eckhaus, M.** and **Bluestone, J. A**. Effects of in vivo administration of anti-CD3 monoclonal antibody on T cell function in mice. II. In vivo activation of T cells. *J. Immunol.* 1989. **142**: 737–743.

24 **Hashimoto, T.** and **Pittet, J. -. F.**, Angiopoietin-2: modulator of vascular permeability in acute lung injury? *PLoS Med.*. 2006. **3**: e113.

25 **Liu, J.**, **Li, S.**, **Liu, J.**, **Liang, B.**, **Wang, X.**, **Wang, H.**, **Li, W.** et al., Longitudinal characteristics of lymphocyte responses and cytokine profiles in the peripheral blood of SARS-CoV-2 infected patients. *EBioMedicine* 2020. **55**, 102763.

26 **Channappanavar, R.** and **Perlman, S.**, Pathogenic human coronavirus infections: causes and consequences of cytokine storm and immunopathology. *Semin. Immunopathol.* 2017. **39**: 529–539.

27 **Takada, H.**, **Takahata, Y.**, **Nomura, A.**, **Ohga, S.**, **Mizuno, Y.** and **Hara, T.**, Increased serum levels of interferon-gamma-inducible protein 10 and monokine induced by gamma interferon in patients with haemophagocytic lymphohistiocytosis. *Clin. Exp. Immunol.* 2003. **133**: 448–453.

28 **Henter, Ji**, **Elinder, G.**, **Soder, O.**, **Hansson, M.**, **Andersson, B.** and **Andersson, U.**, Hypercytokinemia in familial hemophagocytic lymphohistiocytosis. *Blood*. 1991. **78**: 2918–2922.

29 **Osugi, Y.**, **Hara, J.**, **Tagawa, S.**, **Takai, K.**, **Hosoi, G.**, **Matsuda, Y.**, **Ohta, H.** et al., Cytokine production regulating Th1 and Th2 cytokines in hemophagocytic lymphohistiocytosis. *Blood*. 1997. **89**: 4100–4103.

30 **Behrens, E. M.**, **Canna, S. W.**, **Slade, K.**, **Rao, S.**, **Kreiger, P. A.**, **Paessler, M.**, **Kambayashi, T.** et al., Repeated TLR9 stimulation results in macrophage activation syndrome–like disease in mice. *J. Clin. Invest.* 2011. **121**: 2264–2277.

31 **Bonville, C. A.**, **Percopo, C. M.**, **Dyer, K. D.**, **Gao, J.**, **Prussin, C.**, **Foster, B.**, **Rosenberg, H. F.** et al., Interferon-gamma coordinates CCL3-mediated neutrophil recruitment in vivo. *BMC Immunol*. 2019. **10**: 14.

32 **Pollenus, E.**, **Malengier-Devlies, B.**, **Vandermosten, L.**, **Pham, T. -T.**, **Mitera, T.**, **Possemiers, H.**, **Boon, L.** et al., Limitations of neutrophil depletion by anti-Ly6G antibodies in two heterogenic immunological models. *Immunol. Lett.* 2019. **212**: 30–36.

33 **Veras, F. P.**, **Pontelli, M. C.**, **Silva, C. M.**, **Toller-Kawahisa, J. E.**, **de Lima, M.**, **Nascimento, D. C.**, **Schneider, A. H.** et al. SARS-CoV-2-triggered neutrophil extracellular traps mediate COVID-19 pathology. *J. Exp. Med.* 2020. **217**: 20201129.

34 **Hartl, D.**, **Krauss-Etschmann, S.**, **Koller, B.**, **Hordijk, P. L.**, **Kuijpers, T. W.**, **Hoffmann, F.**, **Hector, A.** et al., Infiltrated neutrophils acquire novel chemokine receptor expression and chemokine responsiveness in chronic inflammatory lung diseases. *J. Immunol.* 2008. **181**: 8053–8067.

35 **Luster, A. D.** and **Leder, P.**, IP-10, a -C-X-C- chemokine, elicits a potent thymus-dependent antitumor response *in vivo*. *J. Exp. Med.* 1993. **178**: 1057–1065.

36 **Luster, A. D.**, **Greenberg, S. M.** and **Leder, P.**, The IP-10 chemokine binds to a specific cell surface heparan sulfate site shared with platelet factor 4 and inhibits endothelial cell proliferation. *J. Exp. Med.* 1995. **182**: 219–231.

37 **Qin, S.**, **Rottman, J. B.**, **Myers, P.**, **Kassam, N.**, **Weinblatt, M.**, **Loetscher, M.**, **Koch, A. E.** et al., The chemokine receptors CXCR3 and CCR5 mark subsets of T cells associated with certain inflammatory reactions. *J. Clin. Invest.* 1998. **101**: 746–754.

38 **Thomas, S. Y.**, **Hou, R.**, **Boyson, J. E.**, **Means, T. K.**, **Hess, C.**, **Olson, D. P.**, **Strominger, J. L.** et al., CD1d-restricted NKT cells express a chemokine receptor profile indicative of Th1-type inflammatory homing cells. *J. Immunol.* 2003. **171**: 2571–2580.

39 **Capucetti, A.**, **Albano, F.** and **Bonecchi, R.**, Multiple roles for chemokines in neutrophil biology. *Front. Immunol.* 2020. **11**: 1259.

40 **Sawant, K. V.**, **Poluri, K. M.**, **Dutta, A. K.**, **Sepuru, K. M.**, **Troshkina, A.**, **Garofalo, R. P.** and **Rajarathnam, K.**, Chemokine CXCL1 mediated neutrophil recruitment: role of glycosaminoglycan interactions. *Sci. Rep.* 2016. **6**: 1–8.

41 **Moore, J. B.** and **June, C. H.**, Cytokine release syndrome in severe COVID-19. *Science*. 2020. **368**: 473–474.

42 **Chen, G.**, **Wu, Di**, **Guo, W.**, **Cao, Y.**, **Huang, Da**, **Wang, H.**, **Wang, T.** et al., Clinical and immunological features of severe and moderate coronavirus disease 2019. *J. Clin. Invest.* 2020. **130**: 2620–2629.

43 **Ruan, Q.**, **Yang, K.**, **Wang, W.**, **Jiang, L.** and **Song, J.**, Clinical predictors of mortality due to COVID-19 based on an analysis of data of 150 patients from Wuhan, China. *Intensive Care Med.* 2020. **46**: 846–848.

44 **De Wit, E.**, **Van Doremalen, N.**, **Falzarano, D.** and **Munster, V. J.**, SARS and MERS: recent insights into emerging coronaviruses. *Nat. Rev. Microbiol.* 2016. **14**: 523–534.

45 **Hansel, T. T.**, **Kropshofer, H.**, **Singer, T.**, **Mitchell, J. A.** and **George, A. J. T.**, The safety and side effects of monoclonal antibodies. *Nat. Rev. Drug Discov.* 2010. **9**: 325–338.

46 **Akwii, R. G.**, **Sajib, M. S.**, **Zahra, F. T.** and **Mikelis, C. M.**, Role of angiopoietin-2 in vascular physiology and pathophysiology. *Cells* 2019. **8**: 471.

47 **Li, F.**, **Yin, R.** and **Guo, Q.**, Circulating angiopoietin-2 and the risk of mortality in patients with acute respiratory distress syndrome: a systematic review and meta-analysis of 10 prospective cohort studies. *Ther. Adv. Respir. Dis.* 2020. **14**. https://doi.org/10.1177/1753466620905274

48 **Le, R. Q.**, **Li, L.**, **Yuan, W.**, **Shord, S. S.**, **Nie, L.**, **Habtemariam, B. A.**, **Przepiorka, D.** et al., FDA approval summary: tocilizumab for treatment of chimeric antigen receptor T cell-induced severe or life-threatening cytokine release syndrome. *Oncologist*. 2018. **23**: 943–947.

49 **Al-Salama, Z. T.**, Emapalumab: first global approval. *Drugs*. 2019. **79**: 99–103.

50 **Tomescu, D. R.**, **Dima, S. O.**, **Ungureanu, D.**, **Popescu, M.**, **Tulbure, D.** and **Popescu, I.**, First report of cytokine removal using CytoSorb® in severe noninfectious inflammatory syndrome after liver transplantation. *Int. J. Artif. Organs* 2016. **39**: 336–340.

51 **Giavridis, T.**, **Van Der Stegen, S. J. C.**, **Eyquem, J.**, **Hamieh, M.**, **Piersigilli, A.** and **Sadelain, M.**, CAR T cell–induced cytokine release syndrome is mediated by macrophages and abated by IL-1 blockade. *Nat. Med.* 2018. **24**: 731–738.

52 **Sterner, R. M.**, **Sakemura, R.**, **Cox, M. J.**, **Yang, N.**, **Khadka, R. H.**, **Forsman, C. L.**, **Hansen, M. J.** et al., GM-CSF inhibition reduces cytokine release syndrome and neuroinflammation but enhances CAR-T cell function in xenografts. *Blood* 2019. **133**: 697–709

53 **Huarte, E.**, **O'connor, R. S.**, **Peel, M. T.**, **Nunez-Cruz, S.**, **Leferovich, J.**, **Juvekar, A.**, **Yang, Y-Ou** et al., Itacitinib (INCB039110), a JAK1 inhibitor, reduces cytokines associated with cytokine release syndrome induced by CAR T cell therapy. *Clin. Cancer Res.* 2020. **26**: 6299–6309

54 **Yeleswaram, S.**, **Smith, P.**, **Burn, T.**, **Covington, M.**, **Juvekar, A.**, **Li, Y.**, **Squier, P.** et al., Inhibition of cytokine signaling by ruxolitinib and implications for COVID-19 treatment. *Clin. Immunol.* 2020. **218**: 108517.

55 **Norelli, M.**, **Camisa, B.**, **Barbiera, G.**, **Falcone, L.**, **Purevdorj, A.**, **Genua, M.**, **Sanvito, F.** et al., Monocyte-derived IL-1 and IL-6 are differentially required for cytokine-release syndrome and neurotoxicity due to CAR T cells. *Nat. Med.* 2018. **24**: 739–748

56 **Stone, J. H.**, **Frigault, M. J.**, **Serling-Boyd, N. J.**, **Fernandes, A. D.**, **Harvey, L.**, **Foulkes, A. S.**, **Horick, N. K.** et al., Efficacy of tocilizumab in patients hospitalized with Covid-19. *N. Engl. J. Med.* 2020. **383**: 2333–2344

57 **Panigrahy, D.**, **Gilligan, M. M.**, **Huang, S.**, **Gartung, A.**, **Cortés-Puch, I.**, **Sime, P. J.**, **Phipps, R. P.** et al., Inflammation resolution: a dual-pronged approach to averting cytokine storms in COVID-19? *Cancer Metastasis Rev.* 2020. **39**: 337–340

58 **Lacroix, M.**, **Rousseau, F.**, **Guilhot, F.**, **Malinge, P.**, **Magistrelli, G.**, **Herren, S.**, **Jones, S. A.** et al., Novel insights into interleukin 6 (IL-6) Cis- and trans-signaling pathways by differentially manipulating the assembly of the IL-6 signaling complex. *J. Biol. Chem.* 2015. **290**: 26943–26953

59 **Cossarizza, A.**, **Chang, H. -. D.**, **Radbruch, A.**, **Acs, A.**, **Adam, D.**, **Adam-Klages, S.**, **Agace, W. W.** et al., Guidelines for the use of flow cytometry and cell sorting in immunological studies (second edition). *Eur. J. Immunol.* 2019. **49**: 1457–1973

Abbreviations: **Ang-2**: angiopoietin-2 · **BAL**: Bronchoalveolar lavage · **CAR**: chimeric antigen receptor · **CD**: cluster differentiation · **CRS**: cytokine release syndrome · **HLH**: hemophagocytic lymphohistiocytosis · **hpi**: hour post injection · **IgG**: immunoglobulin gamma · **qPCR**: quantitative polymerase chain reaction

Full correspondence: Walter G. Ferlin, Light Chain
Bioscience-Novimmune S.A., Chemin du Pré-Fleuri 15, 1228
Plan-Les-Ouates, Geneva, Switzerland
e-mail: walter.ferlin@lightchainbio.com

Received: 15/1/2021
Revised: 23/3/2021
Accepted: 28/4/2021
Accepted article online: 4/5/2021

